Journal of Molecular Structure 1052 (2013) 112–124

Contents lists available at ScienceDirect

Journal of Molecular Structure

journal homepage: www.elsevier.com/locate/molstruc

Proficient synthesis of biologically active pregnane derivatives and its glycoside – Experimental and theoretical approach

Arun Sethi [a,*], Akriti Bhatia [a], Atul Maurya [a], Anil Panday [a], Gitika Bhatia [b], Atul Shrivastava [b], Ranvijay Pratap Singh [a], Rohit Prakash [a]

[a] Department of Chemistry, University of Lucknow, Lucknow 226007, India
[b] Division of Biochemistry, Central Drug Research Institute, Lucknow, India

HIGHLIGHTS

- Synthesis of a novel pregnane glycoside is described. All the reaction products were synthesized in a single step reaction.
- Structures of synthesized compounds were established on the basis of their physical, chemical and spectral analysis (UV–Vis, 1H NMR, MS and IR).
- Experimental 1H NMR chemical shifts and IR frequencies were compared with the theoretical values.
- Chemical reactivity of the reactants studied with the aid of reactivity descriptors.
- The newly synthesized compounds were screened for anti-dyslipidemic and anti-oxidant activity.

ARTICLE INFO

Article history:
Received 18 April 2013
Received in revised form 24 August 2013
Accepted 24 August 2013
Available online 30 August 2013

Keywords:
Pregnanes
^{1}H NMR
TD-DFT
Reactivity descriptors
Lipid lowering
Anti-oxidant activity

ABSTRACT

Synthesis of a number of pregnane derivatives including the glycoside has been described in detail. These compounds were synthesized by reaction of 3β-acetoxy-5, 16-pregnadiene-20-one, derived from diosgenin and then treating it with different nucleophilic reagents. The structures of these newly synthesized compounds were established on the basis of their physical, chemical and spectral data. The molecular geometry of compounds were calculated in ground state by density functional theory method (DFT/B3LYP) using 6-31G (d,p) basis set. ^{1}H NMR chemical shifts were also studied using gauge-including atomic orbital (GIAO) approach, which were found in good agreement with the experimental values. The study of electronic properties such as UV–Vis spectral analysis, HOMO and LUMO energy calculations were performed with time dependent DFT (TD-DFT). Global and local reactivity descriptors were calculated to study the reactive sites within the molecules. These compounds were also evaluated for their anti-dyslipidemic (Triton model) and in vitro anti-oxidant activities. Out of these, compound **9** showed potent anti-dyslipidemic and anti-oxidant activity.

1. Introduction

Pregnanes are one of the most versatile steroidal derivatives, which have been dynamically studied. No other group of steroidal derivates has exhibited such a vast range of biologically activity as exhibited by pregnanes [1]. In fact synthesis of pregnane derivatives has attracted the attention of number of research groups belonging to different branches of science and technology [2].

Synthesis of a number of allopregnanolone and pregnanolone analogues exhibiting significant GABA receptor binding property has added a new dimension to the synthetic organic chemistry [3]. A series of novel 2β-piperazino-(20R)-5α-pregnane-3α, 20-diol N-derivatives were evaluated as anti-leukemic agents [4]. Synthesis of a number of C-20 amino, nitro, hydroxyl, oxime and amidinohydrazone derivatives of pregnanes eliciting digitalis like activity have also been reported [5]. D-ring substituted 1,2,3-triazolyl 20-keto pregnane derivatives exhibiting significant anti-cancer activity and were found to be active against DU-145 and PC-3 cell lines [6]. A series of steroid based trioxanes have also been synthesized and evaluated for their anti-malarial activity [7]. Out of these, pregnane based trioxanes showed better activity profile than trioxanes derived from cholesterol and tigogenin. Besides this, a number of 20-oximo pregnane derivatives have been evaluated as inhibitor of human testicular 17α-hydroxylase/$C_{17,20}$-lyase ($P_{450}17\alpha$), thereby preventing the development and progression of benign prostatic hypertrophy and prostatic cancer [8–10]. More recently a number of chalcone pregnenolones were found to possess significant antimicrobial activity [11]. Besides this the requisite side chain of loteprednol etabonate, a corticosteroid used for

* Corresponding author. Tel.: +91 9415396239.
E-mail address: alkaarunsethi@rediffmail.com (A. Sethi).

0022-2860/$ - see front matter © 2013 Elsevier B.V. All rights reserved.
http://dx.doi.org/10.1016/j.molstruc.2013.08.048

anti-inflammatory and allergy related ophthalmic disorders has been introduced in the 16 DPA moiety [12]. In continuation of our synthesis and isolation of some novel pregnane derivatives [13,14] and taking into account the biological importance of these derivatives, we herein report the synthesis, characterization, lipid lowering and anti-oxidant activity of newly synthesized pregnane derivatives **4, 5, 7, 8, 9, 10** supported by theoretical studies. A detailed study regarding the structural and spectroscopic properties of these newly synthesized pregnanes helped in better understanding the chemical reactivity of these compounds. Based on the optimized geometries, the HOMO–LUMO orbitals of **4, 5, 7, 8, 9,** and **10** were generated using TD-DFT approach. Though few papers related to the Density Functional Theory of steroids [15] are available, but not much literature is devoted to theoretical study of pregnanes for evaluating the global and local reactivity descriptors [16]. This prompted us to undertake a detailed chemical reactivity study for better understanding the chemical behavior and predicting the stability and activity of newly synthesized pregnanes.

2. Experimental

2.1. Materials and methods

All solvents used were of laboratory grade and were purified and dried according to standard procedures prior to their use. Thin layer chromatography (TLC) on Silica Gel 'G' (Qualigen, India) coated plates were used for monitoring the progress of reaction and purity of the compounds. Column chromatography was performed using silica gel (60–120 mesh) (Acme, India) as stationary phase. ^{1}H and ^{13}C nuclear magnetic resonance (NMR) spectra were recorded on either Advance FT NMR (400 MHz) (^{13}C, 100 MHz) or Advance DRX (300 MHz) (^{13}C, 75 MHz) or Advance DPX FT (200 MHz) (^{13}C, 50 MHz) (Bruker, Switzerland) using TMS as an internal reference. Fast Atom Bombardment (FAB-MS) was recorded on JEOL SX 102/DA 6000 (Jeol, Japan), using m-nitro benzyl alcohol as matrix (The matrix peak appeared at *m/z* 136, 137, 154, 289 and 307) whereas Electronspray ionization (ESI-MS) was recorded on MICRO-MASS QUATTRO II triple quadrupole (Microcass Altricem, United Kingdom) mass spectrometer. Optical rotations were recorded on SEPA-300 digital polarimeter (Horiba, Japan). IR spectra were recorded on Perkin Elmer FTIR spectrometer with the range from 4000 to 400 cm^{-1}. The spectra were analyzed using Spectrum™ Software suite. The spectra were measured with 4 cm^{-1} resolution and 1 scan co-addition. The ultraviolet absorption (UV) spectra was examined in the range 200–600 nm using a ELICO BL-200 UV–Vis spectrophotometer equipped with a 10 mm quartz cell in chloroform. Melting points were determined in open capillary tubes and were uncorrected. Triton WR-1339 was purchased from sigma chemical company, St. Louis, MO, USA. TG test kits and Total cholesterol test kits were purchased from Merck.

2.2. Synthesis of pregnane derivatives (**1–10**)

The compounds **1–10** were synthesized as given in (Scheme 1).

2.2.1. 3β-Acetoxy-5, 16-pregnadiene-20-one (**1**)

Diosgenin was converted into compound **1** by reported method [17] and identified [18] by its m.p. 168 °C, ^{1}H NMR and ESI-MS.

2.2.2. 3β-Hydroxy-5, 16-pregnadiene-20-one (**2**)

Deacetylation of compound **1** by zemplen method [19] yielded compound **2**, identified by its m.p. 214 °C (lit m.p. 216 °C) [12]^{1}H NMR and ESI-MS.

2.2.3. 3β-Acetoxy-5, 16-pregnadiene-20-one oxime (**3**)

Compound **1** was converted into compound **3** by reported method [20] and was identified by its m.p. 226 °C, ^{1}H NMR and ESI-MS.

2.2.4. 20-(O-2-bromo ethyl)-oximino-3β-hydroxy-pregn-5, 16-diene (**4**)

Compound **3** (500 mg, 1.40 mmol), NaH (96 mg, 4.01 mmol) in dry tetrahydrofuran (THF) (25 mL) was stirred at 0 °C for 30 min. To the reaction mixture 1,2-dibromoethane (0.5 mL) was added and the reaction mixture was further stirred at room temperature for 4 h (the reaction was monitored by TLC during this period). After the reaction was complete, THF was evaporated under reduced pressure and the solid residue obtained was extracted with chloroform, washed with water, dried over anhydrous sodium sulphate and concentrated in vacuum. Column chromatography of the resultant residue afforded (325 mg, 65% yield) compound **4** as syrupy solid. $[\alpha]_D$ – 30° ($CHCl_3$), ^{1}H NMR (300 MHz,$CDCl_3$) δ (ppm) 5.77 (m, 1H, H-16), 5.38 (m, 1H, H-6), 4.60 (m, 2H,=NOC$\underline{H_2}$), 3.94 (m, 2H, C=N—OCH_2C$\underline{H_2}$), 3.58 (m, 1H, H-3), 2.03 (s, 3H, CH_3-21), 1.03 (s, 3H, 19-CH_3), 0.84 (s, 3H, 18-CH_3); ^{13}C NMR (75 MHz, $CDCl_3$), δ171.44 (C-20), 159.94 (C-17), 152.22 (C-16), 142.80 (C-5), 123.41 (C-6), 73.86 (=NO—$\underline{C}H_2$), 71.97 (C-3), 57.63 (C-14), 53.46 (C-9), 45.67 (C-13), 42.71 (C-4), 39.36 (C-12), 37.63 (C-1), 36.22 (C-10), 35.72 (=NO—$CH_2\underline{C}H_2$Br), 34.28 (C-15), 32.63 (C-8), 31.28 (C-7), 29.75 (C-2), 22.93 (C-11), 19.62 (C-19), 17.88 (C-21), 14.77 (C-18); MS *m/z* = 435 [M^+], 437 [M^++2], 388 [435-2CH_3—OH], 295 [435-CH_2CH_2Br—H_2O—CH_3], 251[435-C_4H_7BrNO—2CH_3], 118 [435-$C_9H_{14}O$—C_4H_7BrNO—CH_3].

2.2.5. 3β-Hydroxy-16α-phenyl-pregn-5-en-20-one (**5**)

400 mg of compound **2** was dissolved in 35 mL of dry THF and then 15 mL of phenyl magnesium bromide (in THF) was added to it. The reaction mixture was stirred at 10 °C for 5 h (The reaction monitored by TLC during this period). After the reaction was complete, THF was removed under reduced pressure and the solid residue obtained was extracted with chloroform, washed with water, dried over anhydrous sodium sulphate and concentrated in vacuum. Column chromatography of the resultant residue afforded (275 mg, 75% yield) white solid. m.p. 70 °C, $[\alpha]_D$ – 23° ($CHCl_3$), ^{1}H NMR (300 MHz,$CDCl_3$) δ (ppm) 7.32–7.11 (m, 5H, Ar H's), 5.37(m, 1H, H-6), 3.85 (m, 1H, H-16), 3.57 (1H, m, H-3), 2.71 (d, 1H, H-17, *J* = 9.2 Hz), 2.03 (s, 3H, CH_3-21), 1.03 (s, 3H, CH_3-19), 0.77 (s, 3H, CH_3-18); ^{13}C NMR (50 MHz, $CDCl_3$), δ208.66 (C-20), 147.21 (C-5), 141.21 (C-1′), 128.9 (C-3′ and C-5′), 127.5 (C-2′ and C-6′), 126.2 (C-4′), 121.67 (C-6), 74.45 (C-3), 72.09 (C-17), 57.82 (C-14), 50.44 (C-9), 46.11 (C-13), 42.63 (C-4), 39.39 (C-10), 37.68 (C-12), 36.94 (C-1), 34.76 (C-16) 32.56 (C-15), 32.39 (C-8), 32.18 (C-7), 31.99 (C-2), 30.10 (C-21), 21.42 (C-11), 19.81 (C-19),14.42 (C-18); MS *m/z* = 392 [M^+], 331 [392-$COCH_3$-H_2O], 332 [392-$COCH_3$-OH] 301 [392-$COCH_3$-H_2O-2CH_3), 285 [392-2CH_3—C_6H_5], 270 [285-CH_3]. Anal. Calc. for $C_{27}H_{36}O_2$: C, 82.62; H, 9.24. Found: C, 82.28; H, 9.36.

2.2.6. 3β-Hydroxy-16α, 17α-epoxypregn-5-en-20-one (**6**)

Compound **1** was converted into compound **6** by reported method [21,22]. It was identified by its m.p. 214 °C (lit m.p 216 °C), ^{1}H NMR and ESI-MS.

2.2.7. 3β, 17α-Dihydorxy-16α-[2(2-hydroxy ethoxy) ethoxy] pregn-5-en-20-one (**7**)

1000 mg of compound **6** was dissolved in 10 mL of freshly distilled diethylene glycol and 1.4 mL of boron trifluoride etherate was added to it. The reaction mixture was stirred at 30 °C for 30 h (reaction was monitored by TLC during this period). Ice-cold solution of sodium bicarbonate was added and the aqueous

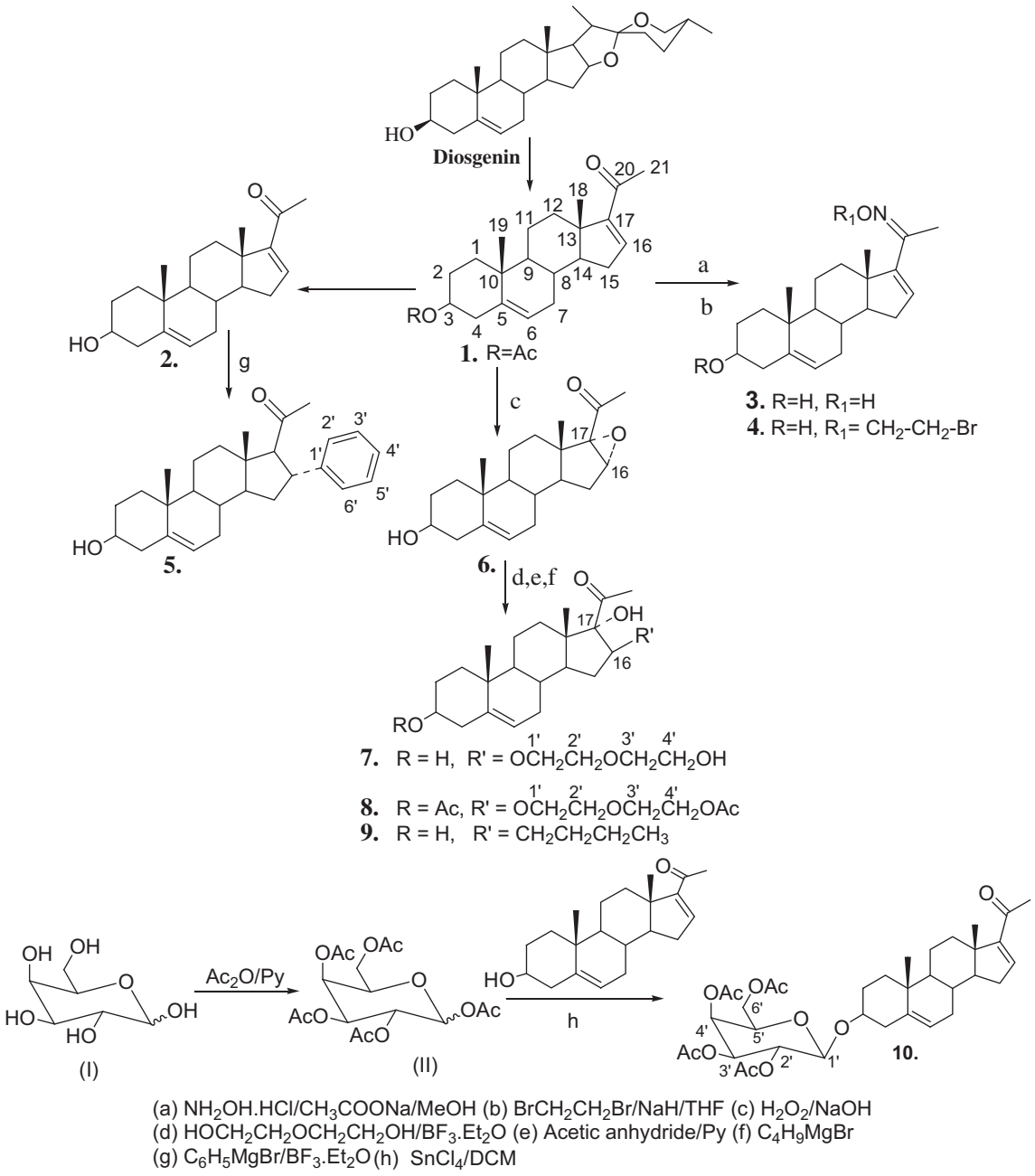

Scheme 1.

phase was extracted with dichloromethane. The organic layer was washed with water, dried over anhydrous sodium sulphate and concentrated in vacuum. The crude product was purified by column chromatography on silica gel (hexane/ethyl acetate 80:20) to afford (852 mg, 85% yield) of compound **7**. m.p. 124 °C, $[\alpha]_D$ – 23° ($CHCl_3$), ^1H NMR ($CDCl_3$,300 MHz) δ (ppm) 5.35 (1H, m, H-6); 4.57 (1H, m, H-16), 3.71–3.65 (6H, m, OCH_2—$C\underline{H}_2$—O—$C\underline{H}_2$—$C\underline{H}_2$—OH), 3.58–3.54 (3H, m, $OC\underline{H}_2$—CH_2—O—CH_2—CH_2—OH, H-3), 2.08 (3H, s, CH_3-21), 1.19 (3H, s, CH_3-19), 0.93 (3H,s, CH_3-18); ^{13}CNMR (75 MHz,$CDCl_3$) δ (ppm) 212.6 (C-20), 141.5(C-5), 121.2(C-6), 96.0 (C-17), 81.4 (C-16), 77.5 (O—CH_2—CH_2—O—$\underline{C}H_2$—CH_2—OH), 72.3 (C-3), 71.7 (O—CH_2—$\underline{C}H_2$—O—CH_2—CH_2—OH), 70.1 (O—$\underline{C}H_2$—CH_2—O—CH_2—CH_2—OH), 65.2 (O—CH_2—CH_2—O—CH_2—$\underline{C}H_2$—OH), 61.4 (C-14), 48.7 (C-9), 42.2 (C-13), 41.9 (C-4), 40.0 (C-12), 36.8 (C-1), 33.1 (C-10), 32.2 (C-15), 31.2 (C-8), 30.5 (C-7), 29.6 (C-2), 28.2 (C-21), 23.6 (C-11), 22.7 (C-19), 19.7 (C-18); MS m/z = 436 [M^+, not observed], 406 [436-2CH_3], 363 [436-$COCH_3$—2CH_3] 346 [363-OH], 347 [436-$COCH_3$-CH_3-CH_2═OH], 331 [436-$OCH_2CH_2OCH_2CH_2OH$], 288 [331-$COCH_3$]. Anal. Calc. for $C_{25}H_{40}O_6$: C, 68.7; H, 9.23. Found: C, 68.22; H, 9.33.

*2.2.8. 3β-acetoxy-17α-hydroxy 16α [2(2-acetoxy ethoxy)-ethoxy] pregn-5-en-20-one (**8**)*

Conventional acetylation of compound **7** with acetic anhydride and pyridine yielded compound **8** as syrupy compound. $[\alpha]_D$ – 30.0°($CHCl_3$), ^1H NMR ($CDCl_3$, 300 MHz) δ (ppm) 5.44 (1H, m, H-6); 5.18 (1H, t, H-16), 4.65–4.59 (3H, m,O—CH_2—CH_2—O—CH_2—$C\underline{H}_2$—OAc and H-3), 4.23–4.14 (4H, m, O—CH_2—$C\underline{H}_2$—O—$C\underline{H}_2$—CH_2—OAc), 3.70–3.64 (2H, m, O—$C\underline{H}_2$—CH_2—O—CH_2—CH_2—), 2.10 (3H, s, CH_3-21), 2.04 (3H, s, OAc), 1.97,(3H, s, OAc), 1.01 (3H, s, CH_3-19), 0.86 (3H, s, CH_3-18); MS m/z = 520 [M^+], 445 [520-CH_3-COOH—CH_3], 385 [520-2CH_3COOH—CH_3].

*2.2.9. 3β, 17α-Dihydorxy-16α-(butyl)-pregn-5-en-20-one (**9**)*

200 mg of compound **6** was dissolved in 20 mL of dry THF and then 5 mL of butyl magnesium bromide (in THF) was added to it. The reaction mixture was refluxed on water bath for 6 h (reaction monitored by TLC during this period). After the reaction was complete THF was removed under reduced pressure and then 100 mL water added to the residue. The reaction mixture was extracted with chloroform thrice. The combined organic extract was dried over anhydrous sodium sulphate and evaporated to dryness. Column chromatography of the residue afforded (150 mg, 75% yield) of compound **9.** m.p. 110 °C, $[\alpha]_D$ – 98° ($CHCl_3$), ^1H NMR ($CDCl_3$, 300 MHz) δ (ppm) 5.35 (1H, m, H-6), 3.53 (1H, m, H-3), 2.25(3H, s, CH_3-21), 2.94 (1H, m, H-16), 1.85–1.60 (6H, m, —C<u>H</u>$_2$—C<u>H</u>$_2$—C<u>H</u>$_2$—), 1.05 (3H, s, CH_3-19), 0.95 (3H, s, CH_3-18), 0.88 (3H, t, —CH_2—CH_3, J = 6 Hz); MS m/z 388 [M^+], 355 [388-H_2O—CH_3], 345 [388-$CH_2CH_2CH_3$], 321 [388-$CH_2CH_2CH_3$—H_2O—CH_3—H], 311[388-CH_2CH_3—H_2O—2CH_3]. Anal. Calc. for $C_{25}H_{40}O_3$: C, 77.27; H, 10.38. Found: C, 76.98; H, 10.44.

*2.2.10. 3β-(2-3, 4, 6-tetra-O-acetyl-β-D-galactopyranosyl)oxy-pregn-5, 16-diene-20-one (**10**)*

Conventional acetylation of D-galactose (2.5 g) with acetic anhydride (12.5 mL) and fused sodium acetate yielded 1,2,3,4,6 penta-O-acetyl-β-D-galactopyranose (II), m.p 136 °C [lit m.p 142 °C]. Stannic chloride (1.0 mL) was added to a solution of 1,2,3,4,6 penta-O-acetyl-β-D-galactopyranose (II) (500 mg) and compound **2** (420 mg) in dichloromethane (20 mL). The mixture was stirred at 20 °C for 4 h under nitrogen condition. The mixture was diluted with dichloromethane and washed with water for decomposition of stannic chloride. The organic layer was washed with 1 M NaOH and water, dried over anhydrous sodium sulphate and then concentrated in vacuum. Column chromatography of the resultant residue afforded (128 mg, 30% yield) compound **10** as syrupy residue. $[\alpha]_D$ – 42.14° ($CHCl_3$), ^1H NMR ($CDCl_3$, 200 MHz) δ (ppm) 6.70 (m, 1H, H-16), 5.44 (1H, m, H-6), 5.07 (dd, 1H, H-2′, J = 8.1 and 3.3 Hz), 5.22 (d, 1H, H-1′, J = 4 Hz), 5.36 (dd, 1H, H-3′, J = 8 and 3.1 Hz), 4.33 (m, 1H, H-4′), 4.28–4.17 (m, 2H, H-6′a and H-6′b), 4.08 (d, 1H, H-5′, J = 7 Hz), 3.90 (m, 1H, H-3), 2.13 (s, 3H, CH_3-21), 2.06 (s, 3H, OAc), 2.03 (s, 3H, OAc), 1.98 (s, 6H, OAc), 1.04 (3H, s, CH_3-19), 0.83 (3H,s, CH_3-18), MS m/z = [M^+] 644 (not observed) 509[644-2CH_3COOH—CH_3], 480[644-2CH_3-COOH—$COCH_3$—H], 393[644-$C_{12}H_{16}O$—CH_3COOH—CH_3], 331 (sugar + 1-OH], 211 [331-2CH_3COOH], 138 [aglycon + 1-$C_{12}H_{16}O$], 120 [120-H_2O], 105 [120-CH_3].

2.3. Lipid lowering and anti-oxidant activity

2.3.1. Experimental animals

Charles Foster strain rats (adult, male) weighing 200–225 g were housed in polyacrylic cages with not more than six animals per cage and maintained under standard laboratory conditions [temperature (25–26 °C), humidity (60–80%) and 12/12 light/dark cycle]. The animals were allowed free access to standard dry pellet diet and water ad libitum. The animals were acclimatized for 10 days before starting the experiment. All the experimental studies were approved by Central drug research institute, ref No. 120/10/Biochem/IAEC) constituted under CPCSEA and GLP annual welfare board, Government of India.

2.3.2. Induction of hyperlipidemia

Adult male rats were divided into nine groups of six rats in each group, namely control (group I), triton treated (group II), triton + **4** (group III), triton + **5** (group IV), triton + **7** (group V) triton + **8** (group VI), triton + **9** (group VII), triton + **10** (group VIII) and triton + Gemfibrozil (100 mg/kg) (group IX). After fasting for overnight, hyperlipidemia was induced in rats of all groups except control group (group I) by single intraperitoneal injection (1 mL/kg) of freshly prepared solution of triton WR-1339 (400 mg/kg) diluted with normal saline solution (400 mg/mL). Animals of all groups were given 0.2% (w/v) aqueous gum acacia suspension orally. The animals of group III, IV, V, VI, VII and VIII were fed orally (10 mL/kg) with compounds **4**, **5, 7, 8, 9** and **10,** macerated with 2% aqueous gum acacia at a dose of 250 mg/kg simultaneously with triton. However group IX, instead of the pregnane derivatives was fed with reference drug-Gemfibrozil macerated with 2% aqueous gum acacia at a dose of 250 mg/kg simultaneously with triton.

2.3.3. Biochemical analysis

After 18 h of fasting, the rats were injected with heparin solution through tail vain at the dose of 1 mL/kg. The animals were anaesthetized with sodium pentothal solution (50 mg/kg, i.p) prepared in normal saline after 15 min of treatment. The blood was withdrawn from retro-orbital sinus with the help of glass capillary coated with EDTA (3 mg/mL blood). The plasma was separated from the blood which was then centrifuged at 4 °C for 10 min. The plasma was diluted with normal saline in the ratio 1:3 (v/v) and further used for TC (Total cholesterol), TG (Triglyceride), PL (Phospholipids) and LCAT (Lecithin-cholesterol-acyl-transferase) assessment using the standard reported protocol [23].

2.3.4. Generation of superoxide anions and hydroxyl radicals

Superoxide anions (O^{-2}) and hydroxyl radicals (·OH) were generated enzymatically by known protocol [1] in the absence or presence of compounds **4, 5, 7, 8, 9, and 10** at concentrations of 100 and 200 (μg/mL). The amount of formazone formed in case of superoxide anions and malondialdehyde (MDA) content in case of hydroxyl radicals generated in both experimental and reference samples were estimated spectrophotometrically at 560 nm [24,25].

2.4. Computational study

The molecular geometry optimization for compounds **1–10** were carried out with Gaussian 03 W [26] program package using B3LYP functional [27] with the standard 6-31G (d,p) basis set. The ^1H NMR isotropic shielding of compounds **4, 5, 7, 8, 9, 10** were calculated with the help of GIAO method [28,29] using B3LYP/6-31G (d,p) method. UV–Vis spectra, electronic transitions and electronic properties such as HOMO–LUMO were further computed with the help of time-dependant DFT (TD-DFT) method. Presentation graphics including visualization of the molecular structures were done with the help of CHEMCRAFT software [30] and Gauss View [31].

3. Result and discussion

3.1. Synthesis

Diosgenin a naturally occurring sapogenin was converted to 3β-acetoxy pregn-5, 16-diene-20-one compound **1** by earlier reported method [17]. Reaction of compound **1** with hydroxylamine hydrochloride in presence of sodium acetate yielded compound **3** [20]. A novel steroidal oximino ether derivative **4** was synthesized by treating compound **3** with 1,2-dibromoethane in dry THF in presence of base NaH [32]. In the ^1H NMR spectrum of compound **4**, two multiplets at δ 4.60 and δ 3.94 are due to methylene groups bonded to oxygen (=N—OC<u>H</u>$_2$) and halogen (C=N—OCH_2C<u>H</u>$_2$Br). In the ^{13}C NMR spectrum the presence of carbon signals at δ 73.86 (=NO—C<u>H</u>$_2$) and δ 35.72 (=NO—CH_2C<u>H</u>$_2$Br) further confirmed the introduction of ethyl group into the oxime **4**. The presence of bands at 1659.0 cm^{-1} for C=N stretching together with a band at 668.31 cm^{-1} for C—Br stretching in the IR spectrum further confirmed the proposed structure. The ESI-MS of compound **4**

Table 1
Effect of compounds **4, 5, 7, 8, 9, 10** on plasma total cholesterol, phospholipids, triglycerides, lecithin cholesterol acyl-transferase levels in triton induced hyperlipidemic rats.

Experimental schedule	Total cholesterol[a]	Phospholipid[a]	Triglyceride[a]	LCAT[b]
Control	85.55 ± 6.70	86.60 ± 5.77	85.80 ± 7.00	65.20 ± 3.88
Triton treated	244.44 ± 20.17*** (+2.95 F)	232.80 ± 16.93*** (+2.62 F)	258.56 ± 20.14*** (+3.01 F)	40.14 ± 2.00*** (−38%)
Triton + **4**	229.99 ± 18.66^{NS} (−6%)	217.27 ± 18.88^{NS} (−7%)	226.66 ± 18.96* (−12%)	40.30 ± 3.12** (+20%)
Triton + **5**	208.33 ± 16.66* (−15%)	189.54 ± 14.82* (−18%)	215.71 ± 18.76* (−17%)	51.84 ± 3.80** (+23%)
Triton + **7**	232.49 ± 19.79^{NS} (−5%)	209.83 ± 17.80* (−10%)	233.09 ± 19.84* (−10%)	52.44 ± 4.00** (+23%)
Triton + **8**	223.05 ± 20.00^{NS} (−9%)	210.56 ± 19.39* (−10%)	235.85 ± 21.22^{NS} (−9%)	43.92 ± 2.77^{NS} (+9%)
Triton + **9**	189.83 ± 13.21** (−22%)	170.25 ± 14.44*** (−26%)	200.95 ± 16.72** (−22%)	58.80 ± 3.80*** (+32%)
Triton + **10**	217.49 ± 18.33* (−11%)	212.39 ± 15.99^{NS} (−9%)	233.66 ± 16.98* (−10%)	48.00 ± 2.77* (+16%)
Triton + Gemfibrozil	158.99 ± 18.33*** (−35%)	160.56 ± 13.20*** (−31%)	177.13 ± 14.00*** (−32%)	61.66 ± 3.92*** (+34%)

Unit: [a]mg/dl, [b]g/dl. Each value is mean ± SD of six rats. $^{*}P\backslash 0.05$, $^{**}P\backslash 0.01$, $^{***}P\backslash 0.001$, NS = non-significant. Triton treated group was compared with control. Triton plus drug and Gemfibrozil treated groups compared with triton only.

Table 2
Effect of compounds **4, 5, 7, 8, 9, 10** on free radical generation (superoxide anions and hydroxyl radicals) in rat liver microsomes in vitro.

Compounds	Dose (μg/mL)	Superoxide anions[a]	Hydroxyl radicals[b]
Control	–	177.29 ± 14.40	104.68 ± 7.89
4	100	EXP 160.43 ± 13.00^{NS} (−9%)	EXP 96.31 ± 8.00^{NS} (−8%)
	200	EXP 154.85 ± 10.62* (−13%)	EXP 88.30 ± 6.11* (−15%)
5	100	EXP 151.59 ± 12.77* (−14%)	EXP 94.48 ± 7.97* (−10%)
	200	EXP 145.24 ± 10.70* (−18%)	EXP 90.78 ± 6.88* (−13%)
7	100	EXP 163.30 ± 15.12^{NS} (−8%)	EXP 97.31 ± 7.77^{NS} (−7%)
	200	EXP 151.33 ± 12.77* (−15%)	EXP 90.11 ± 6.84* (−14%)
8	100	EXP 168.79 ± 14.12^{NS} (−5%)	EXP 97.51 ± 8.12^{NS} (−7%)
	200	EXP 154.79 ± 14.00* (−12%)	EXP 92.44 ± 6.82* (−13%)
9	100	EXP 150.34 ± 12.12* (−15%)	EXP 89.60 ± 6.84* (−14%)
	200	EXP 125.33 ± 10.00*** (−29%)	EXP7 6.22 ± 5.30*** (−27%)
10	100	EXP 161.55 ± 13.66^{NS} (−9%)	EXP 96.00 ± 5.79^{NS} (−8%)
	200	EXP 153.33 ± 11.20* (−14%)	EXP 88.40 ± 4.70* (−15%)
Standard drug	–	57.32 ± 3.84*** (−68% over control) (Allopurinol) (20 μg/mL)	42.81 ± 1.88*** (−59% over control) (Mannitol) (100 μg/mL)

Units: [a]nmol uric acid formed/min; [b]nmol formazone formed/min. Each value is the mean ± SD. $^{*}P\backslash 0.05$, $^{**}P\backslash 0.01$, $^{***}P\backslash 0.001$, NS = non significant as compared to the systems without drug treatment.

recorded the molecular ion peak for Br^{91}at *m*/*z* 437. The fragment at *m*/*z* 295 obtained due to loss of side chain at C-17 followed by loss of methyl radical confirmed the introduction of ethyl bromide group into the oxime. The RDA fragmentation due to Δ^5 bond yielded fragments, which after the loss of side chain at C-17 followed by loss of methyl radical gave fragment at *m*/*z* 118. The formation of this fragment proved the presence of oximo ethyl derivative at C-20.

Synthesis of C-16 substituted pregnane derivative **5** was carried out by treating compound **2** with phenyl magnesium bromide in dry THF. In the ^{1}H NMR of compound **5**, the absence of vinylic proton signal of C-16, together with presence of one proton multiplet at δ 3.85 due to C-16 methine proton and a five proton multiplet from δ 7.32 to δ 7.11 due to aromatic protons suggested the introduction of aromatic ring at C-16. Besides this, the presence of one proton doublet at δ 2.71 presumably due to C-17 proton confirmed the introduction of this group at C-16. The magnitude of the coupling of C-17 proton doublet (J = 9.2 Hz) due to $J_{16\beta H\text{-}17\alpha H}$ confirms the orientation of the side chain at C-16 to be α. In the ^{13}C NMR spectrum the presence of carbon signals at δ 141.2 (C-1′), δ 128.9 (C-3′ and C-5′), δ127.5 (C-2′ and C-6′), δ 126.2 (C-4′), δ 72.0 (C-17), together with the aromatic C—H stretching at 3027.1 cm^{-1} and C=C-C aromatic ring stretching at 1601.8 and 1493.9 cm^{-1} in the IR spectrum, and the fragments at *m*/*z* 331, *m*/*z* 301 and *m*/*z* 285 in the ESI-MS spectra further confirmed the proposed structure.

Epoxides are versatile organic tools as both building blocks and synthetic intermediates. Reaction of compound **6** with diethylene glycol in presence of $BF_3.Et_2O$ led to the formation of compound **7**. The ^{1}H NMR spectrum of compound **7** showed the presence of a broad multiplet of six protons from δ 3.71 to δ 3.65 due to C-4′, C-3′ and C-2′ methylene protons, a three proton multiplet from δ 3.58 to δ 3.54 due to C-1′ methylene and C-3 methine proton along with a one proton multiplet at δ 4.57 due to methine proton at C-16 suggested the introduction of side chain at C-16. In the ^{13}C NMR spectrum of compound **7** the presence of carbon signals at δ 96.0 (C-17), δ 81.4 (C-16), δ 77.5 (C-3′), δ 71.7 (C-2′), δ 70.1(C-1′) and δ 66.0 (C-4′), together with the bands at 1150.5, 1053.5 and 982.0 cm^{-1} for C—O—C stretching, C—O stretching vibration for primary alcoholic group and rocking vibration for methyl respectively further proved the proposed structure. The ESI-MS of compound **7** did not record the M^+ or the protonated molecular ion peak, but the fragment at *m*/*z* 346 and *m*/*z* 331 definitely proved the presence of tertiary hydroxyl group at C-17 and a 2(2-hydroxy-ethoxy) ethoxy group at C-16.

Acetylation of compound **7** with acetic anhydride and pyridine gave the expected diacetyl derivative **8**. In the ^{1}H NMR spectrum of compound **8** the downfield shifting of C-3 methine proton and C-4′ methylene protons of the side chain at C-16, which appeared as multiplet from δ 4.65 to δ4.59 along with the appearance of two

Table 3
Percentage activity change (anti-hyperlipidemic and anti-oxidant) with changes in structural features of compound **1, 4, 5, 7, 8, 9, 10.**

	Percentage activity change (Anti-hyperlipidemic and anti-oxidant)						Structural features
	TC (%)	PL (%)	TG (%)	LCAT (%)	Superoxide anions	Hydroxyl radicals	
1	−4	−10	−4	13	−6%, −12%	−6%, −10%	C═O at C-20, Double bonds at C16-C17 and C5-C6
4	−6	−7	12	20	−9%, −13%	−8%, −15%	C═N at C-20, Double bonds at C16—C17 and C5—C6
5	−15	−18	−17	23	−14%, −18%	−10%, −13%	C═O at C-20, Phenyl ring at C-16, Double bond at C5—C6
7	−5	−10	−10	23	−8%, −15%	−7%, −14%	C═O at C-20, C—O—C linkage at C-16, Double bond at C5—C6
8	−9	−10	−9	9	−5%, −12%	−7%, −13%	C—O—C linkage at C-16 and acetate group at C-3 and C-16 side chain, C═O at C-20, Double bond at C5—C6
9	−22	−26	−22	32	−15%, −29%,	−14%,−27%	Butyl side chain at C-16, C═O at C-20, Double bond at C5—C6
10	−11	−9	−10	16	−9%, −14%	−8%, −15%	C-3 glycoside

singlets of three proton each at δ 2.04 and δ 1.97, suggested the diacetyl nature of compound **8**.

Reaction of epoxide with n-butyl magnesium bromide in dry THF resulted in the formation of compound **9**. In the ^{1}H NMR spectrum of compound **9**, a three proton triplet at δ 0.88 (J = 6 Hz) along with a broad multiplet of six protons from δ 1.85 to 1.60 due to methylene groups of the side chain suggested the introduction of the butyl group. The ESI-MS recorded the molecular ion at m/z 388, besides this the fragment at m/z 345 and m/z 321 due to loss of side chain at C-16 further proved the proposed structure.

Conjugating the pregnane with appropriate carbohydrate moiety not only increases their hydrophilic character but it also increases it efficacy and reduced toxicity relative to the parent pregnane [33]. In our effort to synthesize some novel pregnane glycoside, condensation of glycosyl donor 1,2,3,4,6 penta-O-acetyl-D-galactose (II) with pregnane genin **2** in the presence of Lewis acid catalyst stannic chloride yielded the product **10**. The ^{1}HNMR of compound **10** not only confirmed that it is a pregnane glycoside but it also helped in ascertaining the configuration of the glycosidic linkage. The anomeric proton was observed as a doublet at δ 5.22 (J = 8.1 Hz). The value of large coupling constant, due to diaxial coupling confirmed the glycosidic linkage to be β. The downfield shifting of one proton multiplet of the methine proton at C-3 centered around δ 3.5 (in the genin) and now appearing at δ 3.90 (in the glycoside) was in conformity with the proposed structure that the sugar was glycosidically linked to C-3 hydroxyl group. The presence of vibrational bands at 1180.0 cm^{-1}, 1040.1 cm^{-1} and 661.8 cm^{-1} corresponding to C—O—C stretch, symmetric C—O stretching and O—C—O deformation for acetyl groups further confirms the conjugation of the acetylated sugar with the pregnane moiety. In the FAB-MS of **10**, fragment at m/z 509 obtained by successive loss of two acetic acid molecules and methyl group, and at m/z 480 obtained by successive loss of two acetic acid molecules and C-17 keto-methyl chain suggested that an acetylated sugar is glycosidically linked to pregnane moiety in compound **10** .

3.2. Anti-hyperlipidemic and anti-oxidant activity

Hypercholesterolemia is an essential risk factor for cardiovascular diseases [23]. When plasma cholesterol exceeds the optimum required level, it results in the development of atherosclerosis and stroke [34]. The treatment of hyperlipidemia reduces cardiovascular events [35]. Furthermore hypercholesterolemia increases oxidative stress by production of endothelial superoxide anions. Therefore both hyperlipidemia and oxidative stress plays an important role in atherogenesis [36,37].

Administration of triton WR-1339 to experimental animals caused significant increase in plasma levels of TC (2.9-fold), PL (2.6-fold) and TG (3-fold) as given in Table 1. Treatment with compounds **4, 5, 7, 8, 10** (dose 250 mg/kg p.o) caused mild decrease in plasma levels of TC, PL and TG by 6%, 7%, 12% in case of **4,** 15%, 18%, 17% in case of **5,** 5%, 10%, 10% in case of **7**, 9%, 10%, 9% in case of **8** and 11%, 9%, 10% in case of **10** when compared to triton. In case of **9** the decrease in plasma levels of TC, PL and TG was 22%, 26%, 22% respectively, which was more significant in comparison to compounds **4, 5, 7, 8, 10**. These data were compared with standard drug Gemfibrozil (dose 100 mg/kg) which showed decrease in plasma levels of TC, PL and TG by 35%, 32% and 31% respectively. Triton causes drastic increase in plasma lipid levels by enhancing activity of 3-hydroxy-3-methyl-glutaryl CoA (HMG-CoA) reductase and also inhibits activity of lipases responsible for hydrolysis of plasma lipids [38,39]. Involvement of LCAT in the regulation of blood lipids is also suggested and it plays a key role in lipoprotein metabolism. The test compounds **4, 5, 7, 8, 9, 10** activated plasma LCAT in hyperlipidemic animals, as a result LCAT converts free cholesterol into cholesteryl ester (a more hydrophobic form of cholesterol), which is then sequestered into the core of a lipoprotein particle, eventually synthesizing the less harmful HDL (High Density lipoprotein). The levels of LCAT were increased by 20% in case of **4**, 23% for **5**, 23% for **7**, 9% for **8** and 16% for **10**. Compound **9** showed a significant increase of 32% in LCAT level as compared to triton treated (Table 1).

The scavenging potential of compounds **4, 5, 7, 8, 9,** and **10** on in vitro generation of oxygen free radical at 100 and 200 μg/mL against formation of O^{-2} and ·OH in enzymatic system was also studied (Table 2). The generation of superoxide anion in an enzymatic system was found to be inhibited by **4** (9%), **5** (14%), **7** (8%), **8** (5%), **9** (15%) and **10** (9%) at a dose of 100 μg/mL and (8%), (10%), (7%), (7%), (14%) and (8%) at a dose of 200 μg/mL respectively. The enzymatic generation of hydroxyl free radicals was also inhibited by **4** (13%), **5** (18%), **7** (15%), **8** (12%), **9** (29%) and **10** (14%) at a dose of 100 μg/mL and (15%), (13%), (14%), (13%), (27%) and (15%) at a dose of 200 μg/mL respectively (Table 2**)**. In case of compound **9**, the inhibition was found to be (29%) at a dose of 100 μg/mL for superoxide ion and (27%) at a dose of 200 μg/mL for hydroxyl free radical generation which again was quite significant. The involvement of hydroxyl free radicals (OH·) has been found to be a major causative factor for peroxidative damage to lipoproteins, which is responsible for inhibition and progression of atherosclerosis in hyperlipidemic subjects [40]. Results of in vitro study suggest that compound **9** showed noteworthy decrease in plasma levels of TC, TG, PL and LCAT thus showing a marked improve in the lipid profile of triton induced hyperlipidemic rats and also possessed anti-oxidant property as it potentially inhibited the in vitro generation of both O^{2-} and OH· free radicals in an enzymatic system at 100 μg/mL and 200 μg/mL concentration. With its anti-oxidant

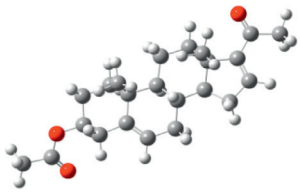

1

E = –1121.44226751 a.u.

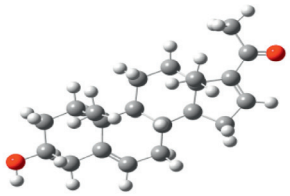

2

E = –968.76655480 a.u.

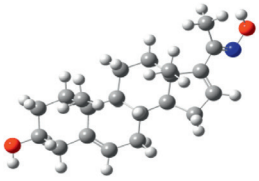

3 E = –1024.05665548 a.u.

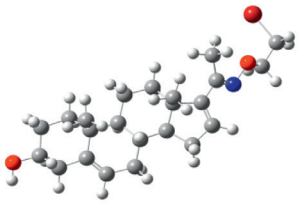

4 E = –3673.79742737 a.u.

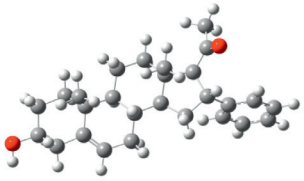

5

E = –1201.05457144 a.u.

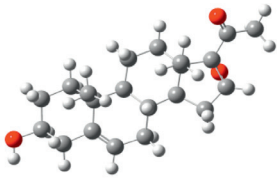

6

E = –1043.97342578 a.u.

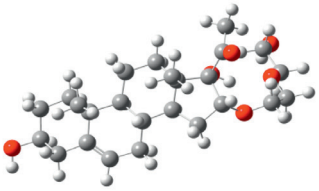

7

E = –1428.10437124 a.u.

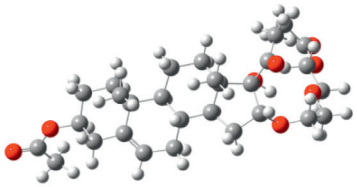

8

E = –1733.42167543 a.u.

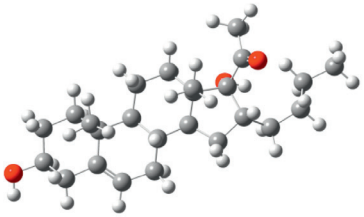

9

E = –1202.47145245 a.u.

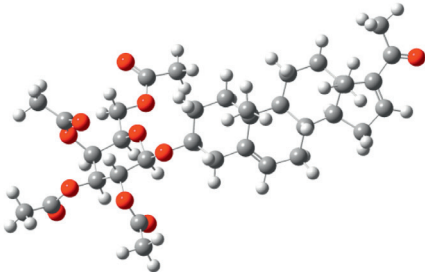

10

E = –2190.17881838 a.u.

Fig. 1. Optimized geometry of compounds **1**–**10** using B3LYP/6-31G(d, p) level of theory.

potential, compound **9** may thus prove to reduce oxidative stress in hyperlipidemic animals thereby preventing occurrence of atherogenic events.

The percentage decrease of lipid parameters (TC, PL, TG) for compound **9** remains to be highest (22%, 26%, 22%) as compared to other compounds indicating that introduction of butyl side

chain at C-16 effects the lipid lowering efficacy of the compound to a greater extent. Similarly, introduction of phenyl ring at C-16 position in compound **5** also causes a significant decrease of all three lipid parameters (15%, 18%, 17%), but this decrease is lower in comparison when butyl is introduced at C-16. However minor decrease in TC, TG and PL levels is observed for compounds **4, 7, 8** and **10**. Similar observations are made regarding decrease in levels of both superoxide and hydroxyl free radicals, where again significant decrease is observed for compound **9**. The structural features responsible for the changes in the anti-hyperlipidemic and anti-oxidant activity taking 16-DPA as the initial moiety (Compound **1**) are summarized in Table 3.

3.3. Molecular structure

The optimized geometries for compounds **1–10** were obtained at B3LYP/6-31G (d,p) level of theory as shown in Fig. 1. All the compounds were in the ground state corresponding to C1 point group symmetry. Conversion of C=O to oxime C=N—OH derivative is evident from the elongation in bond length from 1.22 Å (C=O) to 1.29 Å (C=N) in compound **3,** because nitrogen is lesser electronegative in comparison to oxygen. Introduction of side chain (Br—CH_2—CH_2—Br) at C-20 position in compound **3** also caused slight increase in N-O bond length corresponding to 1.38 Å (C=N—O—H) in compound **3** to 1.40 Å (C=N—O—CH_2—CH_2—Br) in compound **4**. The introduction of phenyl group at C-16 position in compound **5** is evident from the conversion of C16—C17 double bond in compound **2** (1.34 Å) to C16—C17 single bond (1.56 Å) in compound **5**. The C—C and C—O bond lengths in compound **6** is 1.49 Å and 1.45 Å which is very much close to the normal C—C and C—O bond lengths generally observed in case of reported oxiranes (C—C = 1.46 Å and C—O = 1.44 Å). However, opening of the oxirane ring led to the introduction of diethylene glycol at C-16 and hydroxyl group at C-17 position in compound **7.** This compound showed an increase in C16—C17 bond length from 1.46 Å to 1.57 Å, and this appears to be due to the opening of the three membered strained epoxide ring, thereby releaving it from angle as well as torsional strain. Similar observation was made in case of compound **8** and compound **9** where the C16—C17 bond length were calculated as 1.57 Å and 1.56 Å respectively. In case of compound **10**, glycosidation at C-3 position also leads to slight increase in C—O bond length now calculated at 1.44 Å, against the bond length observed for the acceptor molecule **2** at 1.42 Å.

3.3.1. ^1H NMR analysis

The Gauge-including atomic orbital (GIAO) ^1H NMR chemical shift calculations of the compounds **4, 5, 7, 8, 9, 10** were made using B3LYP method in conjugation with 6-31G (d,p) basis set [29]. The experimental and calculated values of ^1H NMR chemical shifts of the newly synthesized compounds **4, 5, 7, 8, 9, 10** are given in Table 4. The correlation between the experimental and calculated ^1H NMR chemical shift values of these compounds are plotted in graphs (**2a–2f**) in Fig. 2. All the six correlation graphs follow the linear equation ($y = mx + c$), where y = theoretical ^1H NMR chemical shift and x = experimental ^1H NMR chemical shift (δ ppm). These graphs shows good correlation between the experimental and the calculated results with the coefficient of regression (R^2) being in the range of 0.97 ≈ 0.99.

Table 4
Comparison between experimental and theoretical ^1H NMR chemical shifts δ (ppm) from TMS for studied compounds **4, 5,7, 8, 9, 10.**

Compounds	Assignment	δ (exp.)	δ (Cacl.)
4	H-16	5.77	6.31
	H-6	5.38	5.45
	=NOC<u>H</u>$_2$	4.60	4.20
	—C=N—OCH$_2$—C<u>H</u>$_2$—Br	3.94	3.58
	H-3	3.58	3.68
	CH_3-21	2.03	2.01
	CH_3-19	1.03	1.14
	CH_3-18	0.84	1.12
5	Ar—H′s	7.32–7.11	7.33–7.11
	H-6	5.37	5.46
	H-16	3.85	3.90
	H-3	3.57	3.72
	H-17	2.71	2.53
	C<u>H</u>$_3$-21	2.03	1.83
	C<u>H</u>$_3$-19	1.03	0.86
	C<u>H</u>$_3$-18	0.77	0.79
7	H-6	5.35	5.40
	H-16	4.57	4.79
	—(O—CH$_2$—C<u>H</u>$_2$—O—C<u>H</u>$_2$—C<u>H</u>$_2$—OH)	3.71–3.65	4.05–3.40
	—(O—C<u>H</u>$_2$—CH$_2$—O—CH$_2$—CH$_2$—OH),	3.58–3.54	3.66–3.21
	H-3		
	CH_3-21	2.08	2.18
	CH_3-19	1.19	1.04
	CH_3-18	0.93	0.65
8	H-6	5.44	5.40
	H-16	5.18	4.79
	—(O—CH$_2$—CH$_2$—O—CH$_2$—C<u>H</u>$_2$—OAc),	4.65–4.59	4.05–3.24
	H-3		
	—(O—CH$_2$—C<u>H</u>$_2$—O—C<u>H</u>$_2$—CH$_2$—OAc)	4.23–4.14	
	—(O—C<u>H</u>$_2$—CH$_2$—O—CH$_2$—CH$_2$—)	3.70–3.64	
	CH_3-21	2.10	2.18
	OAc	2.04	2.01
	OAc	1.97	1.92
	CH_3-19	1.01	1.04
	CH_3-18	0.86	0.62
9	H-6	5.35	5.40
	H-3	3.53	3.69
	CH_3-21	2.25	2.27
	H-16	2.94	3.35
	—(CH_2—CH_2—CH_2)	1.85–1.60	1.68–1.15
	CH_3-19	1.05	1.07
	CH_3-18	0.95	0.73
	—(CH_2—CH_3)	0.88	0.93
10	H-16	6.70	7.28
	H-6	5.44	5.51
	H-3′	5.36	5.87
	H-1′	5.22	5.76
	H-2′	5.07	5.30
	H-4′	4.33	4.53
	H-6′	4.28–4.17	4.05–3.92
	H-5′	4.08	3.85
	H-3	3.90	3.46
	C<u>H</u>$_3$-21	2.13	2.00
	C<u>H</u>$_3$-19	1.04	1.13
	C<u>H</u>$_3$-18	0.83	1.09

3.4. IR analysis

The selected experimental and calculated vibrational wavenumbers along with the corresponding vibrational assignments for compound **4, 5, 7, 8, 9** and **10** are given in Table 5**.** Any discrepancy observed between the experimental and the theoretical values may be attributed to the fact that the experimental results corresponds to solid phase, whereas the theoretical results belong to gaseous phase. In order to obtain good correlation between the two values, the calculated harmonic frequencies were scaled down via scaling factor 0.9608 [41]. In the IR spectrum of compound **4**, the presence of a broad band in the region

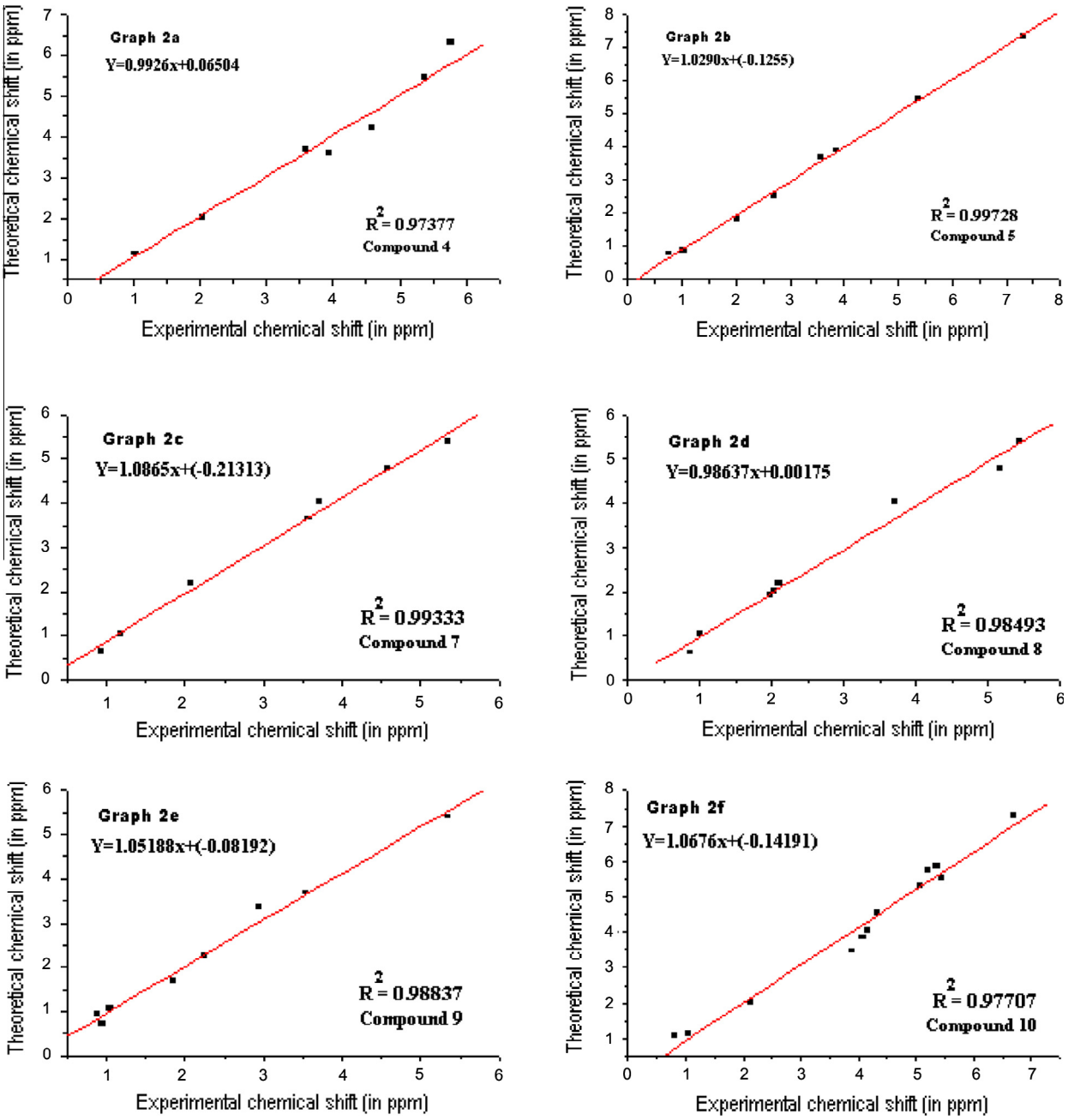

Fig. 2. Linear regression graphs for compound **4** (**2a**), compound **5** (**2b**), compound **7** (**2c**), compound **8** (**2d**), compound **9** (**2e**) and compound **10** (**2f**) between the experimental and theoretical ^{1}H NMR chemical shifts at B3LYP/6-31G.

3600–3400 cm^{-1} for hydrogen bonded OH group centered around 3405.2 cm^{-1} was seen in the spectrum corresponding to the calculated value at 3129.7 cm^{-1}. The characteristic C=N and N—O stretching vibrations of oxime are observed at 1659.0 cm^{-1} and 1045.3, 962.1 cm^{-1}, with the corresponding theoretical values at 1672.1 cm^{-1} and 1039.2, 974.5 cm^{-1} respectively [42]. The band for C—Br stretch is observed at 668.3 cm^{-1} with the calculated value at 692.7 cm^{-1}. In the IR spectrum of compound **5**, the carbonyl group stretch is observed at 1702.3 cm^{-1} along with the bands observed at 3027.1 cm^{-1}, 1601.8 cm^{-1} and 1493.9 cm^{-1} corresponding to C—H aromatic stretch and C=C aromatic stretch respectively. The IR spectrum of compound **7** showed the characteristic stretching vibrations for C—O—C stretching at 1150.0 cm^{-1} with the calculated value being at 1162.0 cm^{-1}, C—O stretching for primary OH at 1053.5 cm^{-1} with the calculated value at 1047.0 cm^{-1} and rocking vibration for methyls at 982.0 cm^{-1} [43] the calculated value being 941.7 cm^{-1}. In addition, the C=O stretch is observed at 1698.5 cm^{-1} along with asymmetric and symmetric C—H stretching vibrations at 2926.6 and 2852.4 cm^{-1} respectively. In the IR spectrum of compound **8**, the corresponding vibrational frequencies for acetate groups are observed at 1242.7 cm^{-1}, 657.5 cm^{-1}, 581.0 cm^{-1} for O=C—O—C stretch, OCO deformation and CCO deformation respectively [44,45]. The calculated values are at 1256.8 cm^{-1}, 653.7 cm^{-1} and 574.9 cm^{-1} respectively. The experimental FT-IR spectrum of compound **9** shows vibrations at 3437.4 cm^{-1},

Table 5
Selected Experimental and Calculated IR frequencies, vibrational assignments for compound **4, 5, 7, 8, 9, 10.**

Calculated IR	Experimental IR	Vibrational assignments
*Compound **4***		
3129.7	3405.2	Hydrogen bonded OH stretch
2961.9	2927.6	Asymmetric C—H stretch
	2856.1	Symmetric C—H stretch
1672.1	1659.0	C=N stretch
1429.2 and 1388.5	1443.8 and 1379.8	CH_3, CH_2 deformation
1039.2	1045.3	N—O stretch
974.5	962.1	
692.7	668.3	C—Br
*Compound **5***		
3137.4	3395.0	Hydrogen bonded OH stretch
3080.8	3027.1	C—H aromatic stretch
2961.7	2926.7	Asymmetric C—H stretch
	2852.6	Symmetric C—H stretch
1795.2	1702.3	C=O stretch
1637.8, 1538.7, 1437.4	1601.8 and 1493.9	C=C—C aromatic ring stretch deformation vibration of methyl of CH_3CO
1393.8	1379.5	
777.1	761.9	CH_2 rocking
*Compound **7***		
3669.7	3406.7	Hydrogen bonded OH stretch
2971.5	2926.6	Asymmetric C—H stretch
	2852.4	Symmetric C—H stretch
1781.0	1698.5	C=O stretch
1396.3	1379.5	Deformation vibration of methyl of CH_3CO
1162.0	1150.0	C—O—C stretch
1047.0	1053.5	C—O stretching vibration for primary OH
941.7	982.0	Rocking vibrations for methyls
*Compound **8***		
3666.8	3417.1	Hydrogen bonded OH stretch
2988.2	2917.9	Asymmetric C—H stretch
	2849.7	Symmetric C—H stretch
1783.1	1733.3	C=O (ester)
1380.4	1373.3	Deformation of methyl of CH_3CO
1256.8	1242.7	O=C—O—C stretch
653.7	657.5	OCO deformation
574.9	581.0	CCO deformation
*Compound **9***		
3134.5	3437.4	Hydrogen bonded OH stretch
2986.4	2931.8	Asymmetric C—H stretch
2961.5	2852.8	Symmetric C—H stretch
1786.3	1701.8	C=O stretch
1441.3	1451.9	CH_3, CH_2 deformation
1392.8	1376.8 and 1355.6	CH_3deformation, CH_2 wagging
1223.2 and 1150.3	1223.9 and 1152.1	CH_3 rocking, CH_2 twisting
*Compound **10***		
2937.5	2924.5	Asymmetric C—H stretch
2882.6	2851.9	Symmetric C—H stretch
1767.0	1728.7	C=O (ester)
1397.4	1377.9	Deformation of methyl of CH_3CO
1169.8	1180.0	C—O—C stretch
1051.8	1040.1	Symmetric C—O stretch
667.8	661.8	O—C—O deformation (acetate)

2931.8 cm^{-1} and 2852.8 cm^{-1} corresponding to hydrogen bonded OH along with both asymmetric and symmetric C—H stretching vibrations. The calculated values corresponds to 3134.5 cm^{-1}, 2986.4 cm^{-1} and 2961.5 cm^{-1} respectively. The vibrational bands observed at 1376.8 cm^{-1} and 1355.6 cm^{-1} corresponds to deformation mode for methyls and wagging vibration for methylenes respectively. Further vibrational bands at 1223.9 cm^{-1} and 1152.1 cm^{-1} corresponds to rocking vibration for methyls and twisting vibration for methylenes respectively [43]. The IR spectrum of compound **10** showed a strong intensity bands at 2924.5 cm^{-1} and 2851.9 cm^{-1} corresponding to asymmetric and symmetric C—H stretch along with a medium intensity band at 1726.7 cm^{-1} for ester C=O respectively. These experimental values showed good correlation with the calculated values. The vibrational bands observed at 1180.0 cm^{-1}, 1040.1 cm^{-1} and 661.8 cm^{-1} corresponds to C—O—C stretch, symmetric C—O stretch and O—C—O deformation for acetate groups of the glycoside with the calculated values being 1169.8 cm^{-1}, 1051.8 cm^{-1} and 667.8 cm^{-1} respectively [46].

Table 6
Experimental wavelengths (nm) and energy (eV) for compounds **4, 5, 7, 8, 9, 10** along with theoretical wavelength (nm) and energy (eV) at TD-DFT/B3LYP/6-31G(d,p).

Compound	Experimental		TD-DFT/B3LYP/6-31G(d,p)	
	λ (nm)	E (eV)	λ (nm)	E (eV)
4	239 and 276	5.1876 4.4922	234 and 250	4.9575 5.2884
5	212	5.8483	208	5.9484
7	220	5.6356	202	6.1356
8	219	5.6614	200	6.1882
9	215	5.7667	204	6.0612
10	239	5.1876	244	5.0644

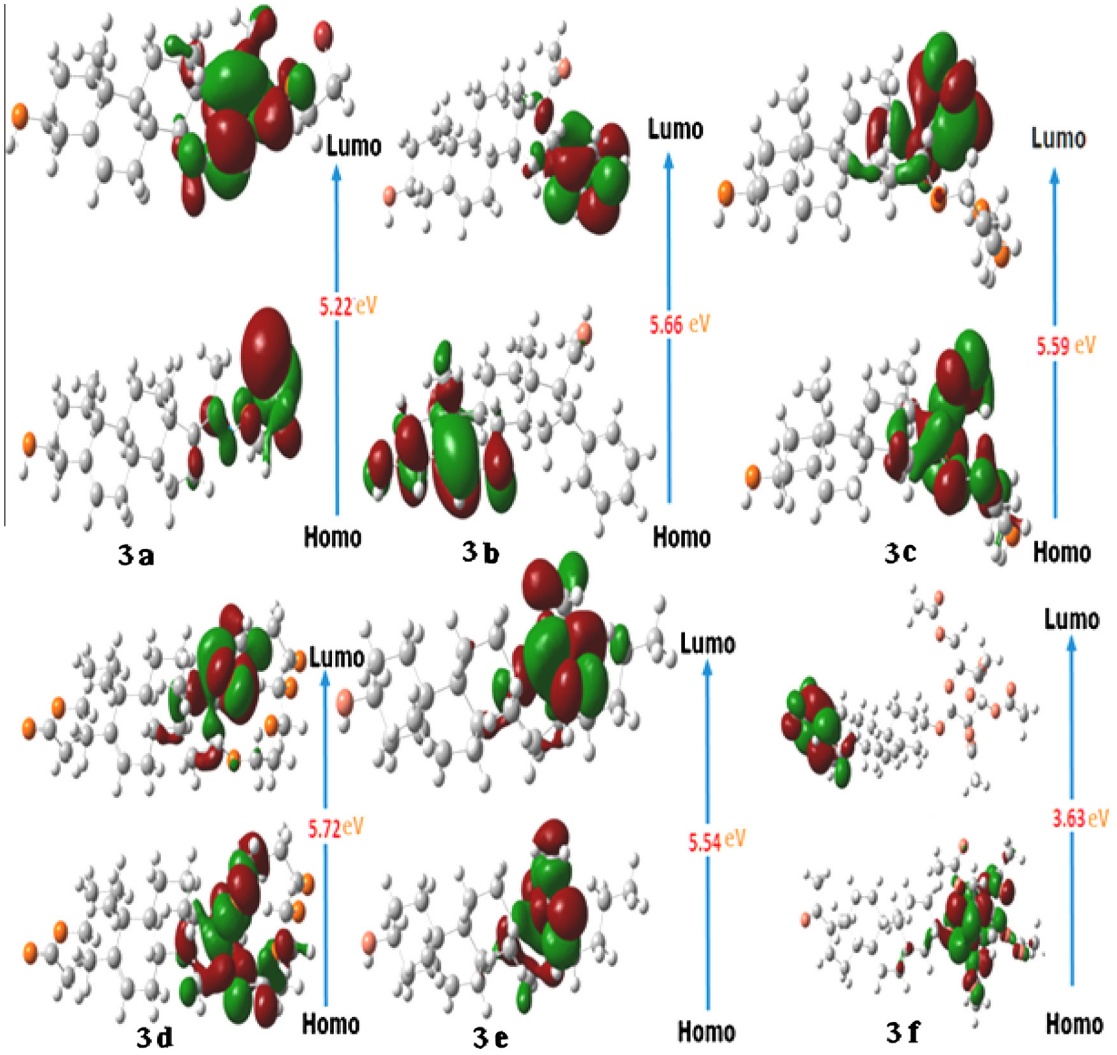

Fig. 3. HOMO–LUMO molecular orbitals depicting the band gap for compound **4** (**3a**), compound **5** (**3b**), compound **7** (**3c**), compound **8** (**3d**), compound **9** (**3e**), and compound **10** (**3f**).

Table 7
Calculated ε_{HOMO}, ε_{LUMO}, energy band gap ($\varepsilon_H - \varepsilon_L$), chemical potential ($\mu$), electronegativity ($\chi$), global hardness ($\eta$), global softness ($S$) and global electrophilicity index (ω) for reactants **2, 3, 6** and products **4, 5, 7, 8, 9, 10** in eV.

Comp.	ε_H	ε_L	$\varepsilon_H - \varepsilon_L$	χ	μ	η	S	ω
2	−6.3213	−1.2515	5.0698	3.7864	−3.7864	2.5349	0.19725	2.8278
3	−5.8987	−0.6721	5.2265	3.2854	−3.2854	2.6133	0.19133	2.0652
6	−6.2606	−0.7725	5.488	3.5166	−3.5166	2.744	0.18221	2.2533
4	−5.9057	−0.6789	5.2268	3.2923	−3.2923	2.6134	0.19132	2.0738
5	−6.1602	−0.4904	5.6698	3.3253	−3.3253	2.8349	0.17637	1.9502
7	−6.1234	−0.5257	5.5977	3.3246	−3.3246	2.7988	0.17864	1.9745
8	−6.3294	−0.6101	5.7193	3.4698	−3.4698	2.8597	0.17485	2.1050
9	−6.1232	−0.5766	5.5465	3.3499	−3.3499	2.7733	0.18029	2.0232
10	−6.2157	−1.3451	4.8706	3.7804	−3.7804	2.4353	0.20531	2.9342

3.5. Electronic absorption

The experimental absorption wavelengths (λ), excitation energies (E), along with the computed values of absorption wavelength (λ) and excitation energies (E) are tabulated in Table 6. The computed values of absorption wavelength (λ), excitation energies (E) and absorbance (A) were studied with the help of TD-DFT approach. Since the FMO's are composed mainly of p-atomic orbitals, therefore these compounds show chiefly π–π^* type transitions. However in case of compound **4**, in addition to a strong band at 239 nm, which is obviously due to π–π^* transitions, another weak band was observed at 276 nm, which arises due to n–π^* transition.

Highest occupied molecular orbital (HOMO) and Lowest unoccupied molecular orbital (LUMO) are one of the important parameters used for predicting the reactivity of compounds. HOMO characterizes the electron donating ability whereas LUMO characterizes the electron accepting ability. The energy gap between HOMO and LUMO called the 'band gap' helps in explaining the eventful charge transfer interaction within the molecule. The 3-D plots of HOMO–LUMO molecular orbitals depicting the band gap

Table 8
Selected electrophilic reactivity descriptors (f_k^+, s_k^+, ω_k^+) and nucleophilic reactivity descriptors (f_k^-, S_k^-, ω_k^-) of reactant **2** and reactant **6** using Hirshfeld atomic charges.

Atom no.	f_k^+	f_k^-	S_k^+	S_k^-	ω_k^+	ω_k^-
Reactant ***2***						
C17	0.0712	0.0179	0.0140	0.0035	0.2013	0.0506
C16	0.1831	0.0513	0.0361	0.0101	0.5177	0.1450
Reactant ***6***						
C17	0.0203	0.0121	0.0037	0.0022	0.0457	0.0273
C16	0.0606	0.0318	0.0110	0.0058	0.1365	0.0718

of compounds **4, 5, 7, 8, 9, and 10** are best illustrated in Fig. 3. In Fig. 3a one clearly sees that the electron density of HOMO is centered on C16—C17 double bond, C=N group and bromine atom while in LUMO the electron density is located around the C16—C17 double bond and the C—20 =N—O group for compound **4**. Similarly, the HOMO orbitals are distributed over C5—C6 double bond and the oxygen of the hydroxyl group at C-3 position, while in LUMO the electron density is mainly located on the phenyl ring in case of compound **5** as seen in Fig. 3**b.** In compound **7,** electron density of HOMO is mainly located over the two oxygen of the side chain and oxygen of the carbonyl group at C-20, whereas LUMO is centered on C-17 carbon and oxygen of $COCH_3$ group seen in Fig. 3**c**. In Fig. 3**d**, the HOMO in case of compound **8** is chiefly distributed over C-15, C-16 and C-17 carbon as well as oxygen's present in the side chain O—CH_2—CH_2—O—CH_2—CH_2—OAc, while the LUMO orbitals can be seen distributed chiefly over C-17 and CO of $COCH_3$. In compound **9**, one sees the HOMO and LUMO orbitals located on C16, C-17 carbons and C=O of $COCH_3$ group as shown in Fig. 3**e**. In Fig. 3**f**, the HOMO orbitals in compound **10**, are centered on oxygen atom of the acetyl groups (O—CO—CH_3) besides carbonyl oxygen of all acetyl groups except that of 6′ position CH_2OAc in compound **10**. LUMO is however mainly concentrated over C16-C17 double bond and C=O of $COCH_3$. The energies of HOMO LUMO orbitals as well as the values for HOMO LUMO band gap energy are given in Table 7.

3.6. Reactivity descriptors

DFT based global and local reactivity descriptors have been extensively used for rationalization and interpretation of diverse aspects of chemical bonding, reaction mechanism and reactive centers. These quantum chemical descriptors are related to electronic structure of compounds and to the mechanism that is involved in the covalent bond formation between the nucleophile and the electrophile. DFT makes it possible to define and well justify different concepts of chemical reactivity. Chemical hardness (η), chemical potential (μ), polarizability (α) and softness (S) [47–51], known as the global reactivity descriptors are used to define the properties of a molecule as a whole, particularly its good electrophilic/nucleophilic nature. Global reactivity descriptors like electronegativity (χ), chemical potential (μ), chemical hardness (η), global softness (S), and global electrophilicity index (ω) were calculated for initial reactants **2, 3,** and **6,** as well as for products **4, 5, 7, 8, 9** and **10** using the energies of frontier molecular orbitals ε_{HOMO}, ε_{LUMO}, which are tabulated in Table 7. Out of the three reactants, reactant **2** acts as a good electrophile as the molecule shows high values for three global reactivity parameters, namely chemical potential (μ) = 3.7864, global electrophilicity index (ω) = 2.8278, and softness (S) = 0.1972 along with the lowest HOMO LUMO energy gap (5.0698 eV), as compared to reactant **3** (ε_H–ε_L = 5.226 eV, μ = 3.285, ω = 2.065, S = 0.1913) and reactant **6** (ε_H–ε_L = 5.488 eV, μ = 3.516, ω = 2.253, S = .1822). The reactant **2** therefore, with high value for all three global reactivity parameters appears to be highly reactive. Similarly, out of the newly synthesized pregnane derivatives **4, 5, 7, 8, 9 and 10**, compound **10** with high values of chemical potential (μ) = 3.780, global electrophilicity index (ω) = 2.934 and softness (S) = 0.2053 also shows its strong electrophilic nature, as a result compound **10** can further be used for the introduction of newer substituent's.

In order to define a particular reactive site within the molecule, local reactivity descriptors such as local softness (S_{ki}), Fukui Function (FF) and local electrophilicity index (ω_k) [50,51] are used. In DFT theory of chemical reactivity, Fukui function $f(r)$ is considered as one of the most fundamental indicator for defining the site selectivity in a given molecular species and for soft–soft type of interactions, the preferred reactive site in a molecule is the one with maximum values of (f_k, s_k, ω_k) [52]. Using Hirshfeld atomic charges of neutral, cation and anion state of initial reactant **2** and **6**, the condensed Fukui functions (f_k^+, f_k^-, f_k^0), local softness (S_k^+, S_k^-, S_k^0) and local electrophilicity indices ($\omega_k^+, \omega_k^-, \omega_k^0$) for atomic sites C-16 and C-17 were calculated and are listed in Table 8. In case of reactant **2** the values of f_k^+, S_k^+, ω_k^+ for two atomic sites C-16 and C-17 are 0.1831, 0.0361, 0.1450 and 0.0712, 0.0140, 0.2013 respectively. Similarly for reactant **6**, the values of local reactivity descriptors f_k^+, S_k^+, ω_k^+ for atomic sites C-16 and C-17 are 0.0606, 0.0110, 0.1365 and 0.0203, 0.0037, 0.0457 respectively. Maximum values of all the three local reactivity descriptors (f_k^+, S_k^+, ω_k^+) in case of both reactant **2** and reactant **6** indicate that C-16 site is more prone for nucleophilic attack in comparison to C-17 atomic site. Therefore, these local reactivity descriptors calculated in case of both reactant **2** and reactant **6**, confirms the favorable site of attack at C-16 position which further leads to the formation of the desired products.

4. Conclusion

Findings from the above study suggest that the reactant **2** was more electrophilic in comparison to other two reactants **3** and **6** and it is for this reason that even after the formation of glycoside **10**, the electrophilicity of the basic pregnane moiety was retained and thus further reaction can be carried out so as to generate more potent biologically active product. Compound **9** showed potent anti-dyslipidemic and anti-oxidant activity. Since this compound possessed an alkyl chain, hence it could be concluded that for further studying the anti-dyslipidemic and anti-oxidant activity, different types of alkyl groups-straight as well branched chain can be introduced at C-16 position.

Acknowledgment

The authors are grateful to the RSIC division of the Central Drug Research Institute, Lucknow for the analytical data.

References

[1] A. Sethi, G. Bhatia, A.K. Khanna, M.M. Khan, A. Bishnoi, A.K. Pandey, A. Maurya, Med. Chem. Res. 20 (2011) 36–46.
[2] R.M. Mohareb, F. Al-Omran, Steroids 77 (2012) 1551–1559.
[3] B. Slavikova, J. Bujons, L. Matyas, M. Vidal, Z. Babot, Z. Kristofikava, C. Sunol, A. Kasal, J. Med. Chem. 56 (2013) 2323–2336.
[4] H. Jegham, R. Maltais, P. Dufour, J. Roy, D. Poirier, Streoids 77 (2012) 1403–1418.
[5] J.F. Templeton, T. Yangzi, T.H. Zaglam, K. Marat, F.S. Labella, J. Med. Chem. 36 (1993) 42–45.
[6] A.H. Banday, A. Shameen, B.D. Gupta, H.M.S. Kumar, Steroids 75 (2010) 801–804.
[7] C. Singh, U. Sharma, G. Saxena, S.K. Puri, Bioorg. Med. Chem. Lett. 17 (2007) 4097–4101.
[8] Y. Ling, J. Li, K. Kato, Y. Liu, X. Wang, C.T. Klus, K. Marat, I.P. Nnane, A.M.H. Brodie, Bioorg. Med. Chem. 6 (1998) 1683–1693.
[9] R.W. Hartmann, H. Hector, S. Haider, P.B. Ehmer, W. Reicher, J. Jose, J. Med. Chem. 43 (2000) 4266–4277.
[10] D.P. Jindal, R. Chattopadhaya, S. Guleria, R. Gupta, Eur. J. Med. Chem. 38 (2003) 1025–1034.

[11] A.H. Banday, M.I. Zargar, B.A. Ganaie, Steroids 76 (2011) 1358–1362.
[12] P. Chowdhury, J.M. Borah, P. Goswami, A.M. Das, Steroids 76 (2011) 497–501.
[13] A. Sethi, A. Bhatia, D. Shukla, A. Kumar, R. Sonker, R. Prakash, G. Bhatia, J. Mol. Struct. 1028 (2012) 88–96.
[14] A. Sethi, S. Paswan, S. Srivastav, N.K. Khare, A. Bhatia, A. Kumar, G. Bhatia, M.M. Khan, A.K. Khanna, J.K. Saxena, J. Asian Nat. Prod. Res. 10 (2008) 1023–1028.
[15] E.V. Rokhina, R.P.S. Suri, Sci Total Enviorn. 417 (2012) 280–290.
[16] R. Parthasarathi, V. Subramanian, D.R. Roy, P.K. Chattaraj, Bioorg. Med. Chem. 12 (2004) 5533–5543.
[17] R.E. Marker, J. Am. Chem. Soc. 71 (1949) 3856–3857.
[18] D.K. Fukushima, T.F. Gallagher, J. Am. Chem. Soc. 73 (1951) 196–201.
[19] A. Sethi, A. Maurya, V. Tewari, S. Srivastava, S. Faridi, G. Bhatia, M.M. Khan, A.K. Khanna, J.K. Saxena, Bioorg. Med. Chem. 15 (2007) 4520–4527.
[20] G. Rosenkrang, O. Mancera, F. Sondheimer, C. Djerassi, J. Org. Chem. 21 (1956) 520.
[21] R. Das, D.N. Kirk, J. Chem. Soc. Perkin Trans. I (1984) 1821.
[22] P. Neher, P. Desaulles, E. Vischer, P. Wieland, A. Wettstein, Helv. Chim. Acta 41 (1958) 1667–1692.
[23] R. Deeg, Ziegehorn, J. Clin. Chem. 29 (1983) 1798.
[24] A. Bindoli, M. Valente, L. Cavallim, Pharmacol. Res. Commun. 17 (1985) 831–839.
[25] B. Halliwell, J.M.C. Gutteridge, O.I. Aruoma, Anal. Biochem. 165 (1987) 215–219.
[26] M.J. Frisch, G.W. Trucks, H.B. Schlegel, G.E. Scuseria, M.A. Robb, J.R. Cheeseman, J.A. Montgomery Jr., T. Vreven, K.N. Kudin, J.C. Burant, J.M. Millam, S.S. Iyengar, J. Tomasi, V. Barone, B. Mennucci, M. Cossi, G. Scalmani, N. Rega, G.A. Petersson, H. Nakatsuji, M. Hada, M. Ehara, K. Toyota, R. Fukuda, J. Hasegawa, M. Ishida, T. Nakajima, Y. Honda, O. Kitao, H. Nakai, M. Klene, X. Li, J.E. Knox, H. P. Hratchian, J.B. Cross, V. Bakken, C. Adamo, J. Jaramillo, R. Gomperts, R.E. Stratmann, O. Yazyev, A.J. Austin, R. Cammi, C. Pomelli, J.W. Ochterski, P.Y. Ayala, K. Voth, G.A. Morokuma, P. Salvador, J.J. Dannenberg, V.G. Zakrzewski, S. Dapprich, A.D. Daniels, M.C. Strain, O. Farkas, D.K. Malick, A.D. Rabuck, K. Raghavachari, J.B. Foresman, J.V. Ortiz, Q. Cui, A.G. Baboul, S. Clifford, J. Cioslowski, B.B. Stefanov, G. Liu, A. Liashenko, P. Piskorz, I. Komaromi, R.L. Martin, D.J. Fox, T. Keith, M.A. Al-Laham, C.Y. Peng, A. Nanayakkara, M. Challacombe, P.M.W. Gill, B. Johnson, W. Chen, Wong, M.W. Wong, C. Gonzalez, J.A. Pople, Gaussian 03, Revision C.02, Gaussian Inc., Wallingford, CT, 2004.
[27] C. Lee, W. Yang, R.G. Parr, Phys. Rev. 37 (1988) 785.
[28] R. Ditchfield, J. Am. Chem. Soc. 93 (1971) 5287.
[29] K. Wolinski, J.F. Hinton, P. Pulay, J. Am. Chem. Soc. 12 (1990) 8251.
[30] G.A. Zhurko, D.A. Zhurko, Chemcraft: Lite Version Build 08 (Freeware), 2005.
[31] Computer program Gauss View 3.09, Ver. 2, Gaussian, Inc., PA. Pittsburgh.
[32] B. Jammart-Gregore, P. Caubere, M. Blank, J.P. Grassounou, C. Advenier, J. Med. Chem. 32 (1989) 315–320.
[33] D.R. Friend, G.W. Chang, J. Med. Chem. 28 (1985) 51–57.
[34] T. Inoue, M. Hayashi, K. Takayanagi, S. Morooka, Artherosclerosis 160 (2002) 369–376.
[35] C.M. Ballantyne, Clin. Cornerstone 8 (2007) S6–S13.
[36] N.G. Stephens, Lancet 347 (1996) 781–786.
[37] Y. Ohara, J. Clin. Invest. 91 (1993) 2546–2551.
[38] M. Kuroda, K. Tanzawa, Y. Tsujita, A. Endo, Biochem. Biophys. Acta 489 (1977) 119–125.
[39] M.C. Schotz, A. Seanu, I.H. Page, Am. J. Physiol. 188 (1957) 399–402.
[40] S. Parthasarathy, D. Steinberg, J.L. Witztum, Annu. Rev. Med. 43 (1992) 219–225.
[41] N. Sundaraganesan, E. Kavitha, S. Sebastian, J.P. Cornard, M. Martel, Spectrochim. Acta A 74 (2009) 788–797.
[42] M. Arivazhagan, S. Jeyavijayan, J. Geethapriya, Spectrochem. Acta A 104 (2013) 14–25.
[43] H.J. Chun, T.L. Weiss, T.P. Devarenne, J. Laane, J. Mol. Struct. 1032 (2013) 203–206.
[44] M. Ibrahima, E. Koglinb, Acta Chim. Slov. 51 (2004) 453–460.
[45] A.P. Ayala, H.W. Siesler, S.M.S.V. Wardell, N. Boechat, V. Dabbene, S.L. Cuffini, J. Mol. Struct. 828 (2007) 201–210.
[46] Z. Mitic, M. Cakic, G.M. Nikolic, R. Nikolic, G.S. Nikolic, R. Pavlovic, E. Santaniello, Carbohydr. Res. 346 (2011) 434–441.
[47] R.G. Pearson, J. Org. Chem. 54 (1989) 1423–1430.
[48] R.G. Parr, R.G. Pearson, J. Am. Chem. Soc. 105 (1983) 7512–7516.
[49] P. Greelings, F.D. Proft, W. Langenaeker, Chem. Rev. 103 (2003) 1793.
[50] R.G. Parr, J. Am. Chem. Soc. 121 (1999) 1922–1924.
[51] P.K. Chattaraj, S. Giri, J. Phys. Chem. A 111 (2007) 11116.
[52] P.K. Chattaraj, S. Giri, S. Duley, Chem. Rev. 111 (2011) PR43–PR75.